sciendo

DOI: 10.2478/auoc-2023-0016

Ovidius University Annals of Chemistry Volume 34, Number 2, pp. 121 - 131, 2023

Comparative analysis of a POPC bilayer and a DPC micelle comprising an interfacial anchored peptide using all-atom MD simulations

Nahuel PERROT[1], Adriana ISVORAN[*,2] Pierre NÉDELEC,[3,4] Nadége JAMIN,[3] and Veronica BESWICK[3,4]

[1]*Department of Medicine, Division of Hematology / Oncology, Beth Israel Deaconess Medical Center, Boston, USA*
[2]*Department of Biology-Chemistry and Advanced Environmental Research Laboratories, West University of Timisoara, Timisoara, Romania*
[3]*Institute for Integrative Biology of the Cell (I2BC), CEA, CNRS, Université Paris-Saclay, F-91191 Gif-sur-Yvette cedex, France*
[4]*University of Evry-val-d'Essonne, Department of Physics, F-91025 Evry, France*

Abstract. Biological membranes are complex systems due to their composition and dynamics. Therefore, membrane mimetics are widely used to investigate lipid properties and interactions between molecules and membrane lipids. Using all-atom molecular dynamics simulations, within this study two systems composed of different membrane mimetics are compared: a 1-palmitoyl-2-oleoyl-3-glycero-phosphatidylcholine (POPC) bilayer or a dodecylphosphocholine (DPC) micelle and a nonapeptide (V94-T-K-Y-W-F-Y-R-L102). Previous ^{1}H-NMR experiments have demonstrated that, in the presence of DPC micelles, this peptide folds as a stable amphipathic helix located in the polar head group region with the tryptophan residue pointing toward the inside of the micelle. The present comparison reveals a hydrophobic surface twice as large for the micelle as for the bilayer and a different arrangement of the acyl chains. The peptide secondary structure is not strongly affected by the membrane mimetics whereas the peptide is more deeply inserted in the bilayer than in the micelle. The contacts between the peptide and the DPC or POPC molecules are analysed and although the distances and lifetimes of these contacts are very different in the micelle and the bilayer, similar specific interactions were found that mainly involved the side chains of the residues R101 and L102.

***Keywords*:** membrane; interactions peptide-lipids; secondary structure; dynamics.

1. Introduction

Biological membranes play a crucial role in living cell. They separate the interior of the cell from the outside environment as well as different compartments within the cell. They are very complex systems composed in part of different types of lipids and membrane proteins. The lipids differ by their head groups, acyl chain number, length and bonds. They arrange to form a bilayer by exposing to the solvent their hydrophilic head groups while their hydrophobic acyl chains are embedded in the core of the bilayer. The membrane proteins are involved in many cellular functions such as signalling, transport, energy transduction and cell adhesion. Biological membranes are also very dynamic systems and numerous interactions take place between their different components.

To overcome the complexity and the heterogeneity of membranes, membrane mimetics are commonly used to investigate lipid properties, membrane protein structure and peptide/protein- membrane interactions [1, 2]. The choice of a membrane mimetic is related to the experimental methodology and/or to the protein to be investigated. Examples of model membranes are giant unilamellar vesicles (GUVs) and liposomes composed of one or few types of lipids as well as micelles of detergent molecules and bicelles. Among the different model membranes, this study focusses on two different systems: a POPC (1-palmitoyl-2-oleoyl-sn-glycero-3-phosphatidylcholine) bilayer and a DPC (dodecylphosphatidylcholine) micelle. As a matter of fact, POPC lipids and DPC molecules are composed of the same zwiterrionic head group and differ by their aliphatic chains (Supplementary Figure S1). POPC lipids comprise two aliphatic chains, a saturated palmitoyl chain (16 carbons) and an unsaturated oleoyl chain (18 carbons) and assemble to form a bilayer. DPC molecules possess only one saturated acyl chain (12 carbons) and form small micelles (when their concentration is above the critical micelle concentration) compatible with different experimental techniques such as high resolution NMR and fluorescence spectroscopies. Therefore, DPC micelles are widely used to solubilise interfacial or hydrophobic peptides and membrane proteins in order to determine their 3D structure [1].

Experiments performed on POPC bilayers and DPC micelles have intended to give a detailed description of these systems. The experimental data obtained for POPC bilayers essentially concern the lipid surface area and volume [3], order parameters [4] as well as

[*] Corresponding author. *E-mail address:* adriana.isvoran@e-uvt.ro (Adriana Isvoran)

orientation of lipid chains and head groups [4]. For DPC micelles, less experimental data are reported in the literature than for POPC as most of the studies concerned DPC-peptide/protein systems and have focused on the inserted peptide or protein. The experimental data available mainly include the micelle shape and the aggregation number [5]. During the past decades, reported molecular dynamics simulations gave new insights into POPC bilayers [4, 6, 7] and DPC micelles [6, 8] such as structural details of acyl chains (dihedral angles and percentage of defects along the chains), the hydrophobic surface, the head group hydration, and the lipid diffusion.

Concerning the interactions between interfacial anchored peptides and POPC bilayers or DPC micelles, most of the experimental studies give atomic description of the peptide structure. Only in few studies, the specific interactions between the peptide and the DPC or POPC molecules are described [9, 10]. Indeed, such experimental information is scarce due essentially to the unfavourable dynamics of the systems, especially at the membrane interface where the dynamics of the lipid head groups is important. On the contrary, molecular dynamics simulations allow an atomic description of the interactions which take place between the peptide and the lipids both for bilayers and micelles [11-14].

Even though POPC bilayers and DPC micelles are widely used, no detailed comparative analysis at the molecular level of these two systems has been performed. Moreover, MD simulations allow such an analysis as well as the detailed structural study of the insertion of a peptide in these membrane mimetics both in terms of structure and interactions with lipids [15].

In the present work, molecular dynamics simulations of two different systems was performed: a POPC bilayer and a DPC micelle in which the same nonapeptide was inserted. The peptide sequence is as follows: V94-T-K-Y-W-F-Y-R-L102, it is a short sequence of the caveolin-1 protein revealing a hydrophobic character [16]. Caveolins are major components of caveolae which are microdomains of the plasma membrane involved in a large number of biological functions, including signal transduction, cholesterol homeostasis and transport [17]. The peptide sequence comprises a cholesterol recognition/interaction motif (V/L-X(1-5)-Y-X(1-5)-R/K, where X(1-5) represents one to five residues of any amino acid), identified by Li et al. [18] and proposed to be involved in the incorporation of proteins into cholesterol-rich domains of membranes [19]. The peptide structure was previously determined from ^{1}H-NMR experiments performed in the presence of DPC micelles [20]. The peptide folds as a stable amphipathic helix which is located in the polar head group region of DPC micelles with the tryptophan residue pointing towards the inside of the micelle.

In this study, a detailed description of the POPC bilayer and the DPC micelle is presented in order to compare the structural characteristics of these two membrane mimetics at the molecular level, taking into account the molecular dynamics simulation outcomes and compared with previously published simulation and experimental data obtained for DPC [21-23] and for POPC respectively [24-26]. Then, this study considers analysis and comparison of the structure and insertion of the nonapeptide in both environments. Finally, the contacts between the peptide and the DPC or POPC molecules are analysed and specific interactions are highlighted.

2. Experimental

2.1. Simulation

The CHARMM program [27] was used for molecular dynamics simulation with the PAR22 [28] and PAR36 [29] all-atom force fields for proteins and for lipids respectively, including parameters for DPC, POPC and the TIP3P water potential [30]. The starting cav-1(94-102) nonapeptide structure was derived from ^{1}H-NMR data obtained for the peptide in the presence of DPC [20]. The structure comprises a single amphipathic helix. The peptide was manually placed at the membrane interface such that it lies parallel to the membrane plane with the tryptophan residue inserted in the hydrophobic core of the membrane according to the experimental data [20].

2.2. Cav-1(94-102) peptide into POPC bilayer

The initial hydrated and equilibrated phospholipid bilayer comprising 242 POPC (121 POPC per layer) was already obtained in a previous study [31]. The fixed dimensions (X, Y, Z) of the primary cell are 88 Å, 88 Å, 90 Å. The X and Y dimensions of the simulation box corresponded to 64 Å^2 for POPC lipid cross-section at 310 K and the Z dimension was chosen such that eight water layers lie on each membrane side which is enough to hydrate the membrane (i.e. 50 water molecules per POPC). The system consisted of 69362 atoms (242 POPC lipids, 12247 water molecules, 2 Cl^- ions to neutralize the system and the nonapeptide). This system was further equilibrated for 5 ns. Production at 310 K with a constant volume and the Leap Verlet algorithm [23] was performed over the course of 50 ns for the POPC bilayer. Electrostatic and van der Waals interactions were truncated at a cut-off distance of 12 Å using a smooth switching function on electrostatic forces and with a shifting function on van der Waals potential over a 4 Å interval (this truncation scheme has been shown to be efficient and accurate in a previous study) [31]. A cut-off distance of 14 Å was used to calculate the non-bonded lists and image lists. Lengths of all bonds involving hydrogen atoms were constrained using the SHAKE algorithm [32], which allows a 2 fs time step to be used for the numerical integration of the equations of motion. Periodic boundary conditions were applied in the three dimensions.

2.3. Cav-1(94-102) peptide into DPC micelle

A DPC micelle was manually constructed starting with 50 monomers of DPC. The monomers were placed such that their polar head-groups formed a spherical interface and their hydrophobic acyl chains were buried inside the sphere. This number of DPC molecules was first estimated by Lauterwein et al. [33] by analytical ultracentrifugation and is in the range of the aggregation number experimentally determined so far (between 44 and 80) [21]. This construction was then equilibrated for 5 ns prior to the insertion of the peptide. The dimensions

(X, Y, Z) of the primary cell were chosen as follows 74.5 Å, 74.5 Å, 74.5 Å. 12413 water molecules were added to the system which is enough to hydrate the micelle (i.e. 248 water molecules per DPC) and ions were finally added to neutralize the system (2 Cl^-). The entire system consisted of 41676 atoms (50 DPC, 12413 water molecules, 2 Cl^- and the nonapeptide) and was further equilibrated for 5 ns. Production was performed over the course of 50 ns under constant temperature (310 K) and constant pressure (1 atm) via Nose-Hoover Langevin piston pressure control (p_{mass} = 50 g mol^{-1} and t_{mass} = 500 kcal mol^{-1} ps^{-2}). The particle mesh Ewald (PME) method [34] was used to compute the long-range electrostatic interactions with a real-space cut-off of 12 Å, a kappa value of 0.34 $Å^{-1}$ and a sixth-order spline. Van der Waals interactions were truncated at a cut-off distance of 12 Å with a switching function on potential over a 4 Å interval. A cut-off distance of 14 Å was used to calculate the non-bonded lists and image lists. We used a dihedral-based correction map [35] for peptide backbone (CMAP) and the SHAKE algorithm [32] to constrain bond vibrations involving hydrogen atoms. The simulation was run with a time step of 2 fs. Periodic boundary conditions were applied to the three dimensions.

2.4. L_{geo}/L ratio

L_{geo}/L ratio was computed for both considered systems. L_{geo} is the length of the acyl chain calculated as the distance from the first carbon of the chain to the last carbon of the chain. *L* is the length of the chain obtained from the addition of all the bond lengths constituting the acyl chain. The L_{geo}/L value obtained for an all-trans chain composed of *n* carbons with a distance *d* between 2 carbons and an angle CCC of 113° is 0.83 as $L_{geo} = (n-1)\, d \sin\left(\frac{113^o}{2}\right)$ and $L = (n-1)d$, thus $\frac{L_{geo}}{L} = \sin\left(\frac{113^o}{2}\right) = 0.83$. The presence of a defect within the chain involves a deviation of the chain direction and a shortening of the chain length computed as the distance from the first to the last carbon. L_{geo}/L slightly decreases (about 0.05) per additional defect in the chain.

2.5. Contact maps

To investigate the chemical environment and the interactions between the nonapeptide and the lipids, the 2-dimensional contact maps were computed. The ox-axis displays selected atoms of the 50 DPC or 121 POPC molecules and the oy-axis displays selected atoms of the peptide residue. The selected atoms for DPC or POPC are: the nitrogen atom (N), the phosphorus atom (P), the glycerol atoms (C1, C2, C3, only for POPC) and the centres of mass of different acyl chain segments. The segments are defined as follows: C21-C26, C25-C210, and C29-C212 for DPC acyl chain; C21-C27, C26-C212 and C211-C218 for oleoyl chain and, C31-C37, C36-C312 and C311-C316 for palmitoyl chain (see Supplementary Figure S1 for DPC and POPC carbon atoms numbering). For the peptide residues, the selected atoms are the centres of mass of each residue side chain. Contacts are characterized by distance and lifetime. Lifetime is correlated to the number of consecutive frames for which the distance criteria is satisfied. A minimum number of three consecutive frames is required to start the count and too short events (< 50 frames over 5000 frames for the whole simulation) were discarded to prevent background noise. Moreover, some leaps are allowed as long as they do not exceed 20 frames. A colour code indicates the range of the contact distance in Å (red: [4.5; 5.5], pink: [5.5; 6.5], blue: [6.5; 7.5], light blue: [7.5; 8.5]). Lifetime range is depicted by the size of the dot and is expressed as a percentage of the total simulation time (small for short lifetime < 15%, medium: [15%; 30%], large: [30%; 50%], very large for long lifetime ≥ 50%).

3. Results and discussion

3.1. Comparative structural and dynamical analysis of lipid systems

The shape of the DPC micelle can be evaluated by calculating the principal inertia moments (I_1, I_2, I_3), the eccentricity defined as [36]:

$$e = \frac{I - I_{min}}{I_{ave}} \qquad (1)$$

where I_{min} is the moment with the minimum value and I_{ave} is the average moment value, and the asymmetry parameter, α, defined as [22]:

$$\alpha = \frac{2I_1 - I_2 - I_3}{I_1 + I_2 + I_3} \qquad (2)$$

A spherical shape would be characterized by inertia moments in the ratio of 1:1:1, e = 0 and α < 0.05. The average moments of the DPC micelle over the course of the simulation are in the ratio of 1.25:1.1:1, e = 0.12 and α = 0.12. These values are concordant with the DPC micelle being a prolate. This is in agreement with previous experimental data [5] and simulation studies [8]. The micelle size, calculated as the mean value of the radius of gyration over the course of the simulation, is 16.1 Å, a value in good agreement with those reported so far [37, 38]. In particular, Cheng *et al.* [37] indicated a slightly higher value of 16.5 Å for a micelle composed of 54 DPC molecules. The size of the hydrophobic core of the micelle was derived from the maximum of the probability distribution of the phosphorus atoms of the DPC head groups with respect to the micelle center of mass (i.e. 18.8 Å), giving a hydrophobic core diameter of 37.6 Å. In comparison, the thickness of the hydrophobic core of the POPC bilayer (defined as the distance between the mean positions of the two phosphorus distributions) is 41 Å.

The orientation of the lipid head groups was studied in both systems. In POPC bilayer, it was computed as the angle formed by the vector joining the phosphorus and the nitrogen atoms ($\overrightarrow{PN}$) and the z-axis. In the DPC micelle, the angle was defined by the vector joining the phosphorus and the nitrogen atoms ($\overrightarrow{PN}$) and the direction of the micelle diameter (vector joining the micelle center of mass and the phosphorus atom). The mean values obtained are 76° and 83° for POPC and DPC respectively indicating that head groups are almost perpendicular to the surface normal i.e. head groups lie parallel to the membrane and micelle surface

respectively. These results are in perfect agreement with experimental and simulation data obtained for bilayers [24, 25] and micelles [21, 22].

The mean position of the different carbons of the acyl chains has been followed during the simulations and presented in Figure 1.

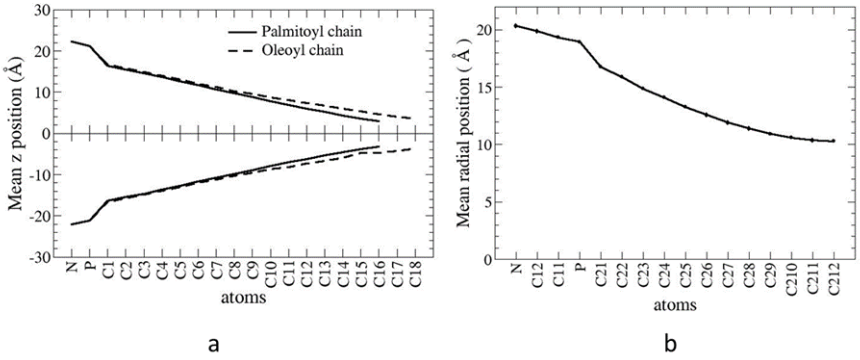

Figure 1. Mean position along z-axis of different atoms of POPC lipids (a) and mean radial position of different atoms of DPC molecules (b) over the course of the simulation. The nitrogen and phosphorus atoms of the head groups are presented as well as the different carbons of the palmitoyl (solid line) and oleoyl (dashed line) chains (a). The nitrogen, the two carbons (C11 and C12) and the phosphorus atoms of the head group are presented as well as the different carbons of the acyl chain (b).

For POPC, the carbons are regularly distributed along the z-axis with the first carbon of the chain situated close to the interface and the last carbon situated at the center of the bilayer (Fig. 1.a). In contrast, the DPC carbon mean positions slowly decrease along the hydrocarbon chain and reach a plateau value around 10 Å revealing that the last carbons of the acyl chain are not buried in the core of the micelle (Fig. 1.b). Moreover, the radial distribution of the last carbons of the chain is broad compared to the first carbons of the chain which display narrow distributions (the standard deviations are 6 Å and 3 Å for the last and first carbons respectively, Supplementary Figure S2). Similar results have been already noticed in the case of a 1.22 ns MD simulation of a DPC micelle comprising 60 molecules and at 300 K [7]. These results reveal a special arrangement of the molecules of DPC within the micelle far from the ideal radial distribution of the detergent molecules constituting the micelle.

To further characterize the acyl chain conformation of DPC and POPC in the micelle and in the bilayer respectively, the dihedral angle distributions were computed (Figure 2).

For the POPC bilayer, the dihedral angle distribution of the palmitoyl and the oleoyl hydrocarbon chains shows that gauche conformations or defects (60° deviation) account for 25% and 29% of total dihedral angles, respectively, whereas for DPC, the percentage of defects is 31% i.e. slightly greater than for the palmitoyl chain. These defects are not uniformly distributed along the hydrocarbon chains as reported in Table 1. All the chains exhibit higher percentage of defects at the beginning and at the end of the hydrocarbon chains. Moreover, the double bond of the oleoyl chain affects the neighboring dihedral angles. For POPC, our results are in accordance with previous experimental data [26] as well as data derived from molecular dynamics simulations [6]. Finally, for our DPC micelle, we found similar results as those reported for a micelle of 54 DPC for which the calculated percentage of defects was 29.3% and, the first and last dihedral angles of the acyl chain were substantially in a gauche state [22].

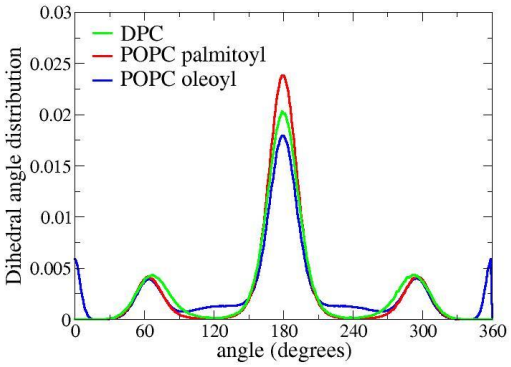

Figure 2. Dihedral angle distributions for the DPC acyl chain (green), POPC palmitoyl (red) and oleoyl (blue) chains over the course of the simulation.

Table 1. Percentage of gauche conformations along the acyl chain of DPC, the palmitoyl and the oleoyl chains of POPC. The dihedral angle is in gauche conformation if the angle is in the range 30°-120° or 240°-330°.

Dihedral angles	DPC	POPC Palmitoyl	POPC Oleoyl
C1-C2—C3-C4	37	32	41
C2-C3—C4-C5	27	35	35
C3-C4—C5-C6	32	23	23
C4-C5—C6-C7	29	23	26
C5-C6—C7-C8	31	21	20
C6-C7—C8-C9	30	22	38

Dihedral angles	DPC	POPC Palmitoyl	POPC Oleoyl
C7-C8—C9-C10	32	21	39
C8-C9—C10-C11	30	23	0
C9-C10—C11-C12	37	23	39
C10-C11—C12-C13		24	40
C11-C12—C13-C14		24	22
C12-C13—C14-C15		25	27
C13-C14—C15-C16		29	24
C14-C15—C16-C17			26
C15-C16—C17-C18			29

The presence of defects modifies the direction of the acyl chain and thus its conformation. Therefore, to gain insights into the different conformations of the acyl chains, the corresponding $^{L_{geo}}/_{L}$ ratios were computed (see Experimental section) and their distributions are presented in Figure 3.

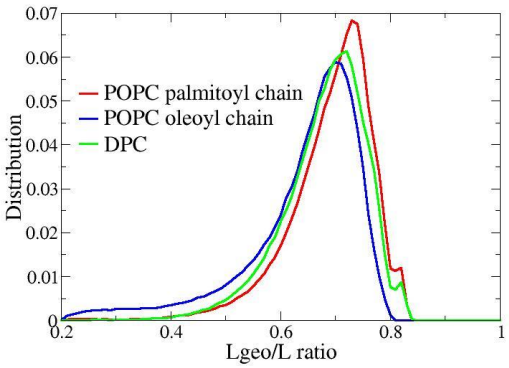

Figure 3. Distributions of $^{L_{geo}}/_{L}$ ratio for the DPC acyl chain (green), POPC palmitoyl (red) and oleoyl (blue) chains over the course of the simulation.

If all the chain dihedral angles correspond to trans conformations, the expected value of $^{L_{geo}}/_{L}$ ratio is 0.83 and this value decreases as the chain bends i.e. when the first and last chain carbons get closer in space. The $^{L_{geo}}/_{L}$ ratios for both DPC and palmitoyl chains exhibit similar profiles: a small population of all-trans conformation, a main distribution centered at about 0.7 and negligible population of conformations with ratio values below 0.5. Palmitoyl chains present more extended conformations and fewer defects (25% versus 31%) than DPC chain leading to a more abundant population of all-trans conformations and to a shift of the maximum of the $^{L_{geo}}/_{L}$ ratio distribution toward higher value, as seen in Figure 3. The presence of the *cis* double bond conformation in oleoyl chain is attested by the absence of the peak characteristic of all-trans population in its $^{L_{geo}}/_{L}$ ratio profile. Moreover, the presence of the *cis* double bond conformation and the numerous defects (29%) are responsible for both the main peak being centered at about 0.7 and an additional distribution of conformations with small $^{L_{geo}}/_{L}$ ratios (from 0.2 to 0.4, Figure 3). The presence of these conformations having very small ratios (from 0.2 to 0.4) reflects the capability of the oleoyl chain to curl around such that its methyl group is close to the first carbon of the chain and thus close to the bilayer interface. These specific conformations have already been described for polyunsaturated acyl chains as “looped shape” [39].

The DPC micelle and the POPC bilayer also differ by the hydrophobicity of their surfaces. As a matter of fact, the hydrophobic surface defined as the acyl chain surface accessible to the solvent using a probe with a radius of 1.4 Å represents 20 % of the total surface of the micelle whereas it represents only 10 % of the total surface of the bilayer. These results obtained for the DPC micelle and the POPC bilayer agree perfectly well with the value of 20.2 % obtained by Abel et al. [23] for a micelle composed of 54 DPC and with the value of 8 % obtained by Lee et al [24] for a POPC bilayer.

3.2. Structural analysis of the peptide

The peptide adopts a stable helical conformation in both simulations as evaluated by the backbone RMSD (1.3 Å). Side-chain RMSD is 3.65 Å and 3 Å in the DPC micelle and the POPC bilayer respectively. This result is in good correlation with published data: (i) other molecular dynamics studies revealed that the antimicrobial peptides SAAP-148 [10] and hylaseptin-4 [13] stabilize their helical conformations when interacting with DPC micelles; (ii) circular dichroism data revealed helical structure for the antimicrobial peptide anoplin when interacting with DPC micelle and POPC:POPG liposomes [40].

The mean position of the peptide α-carbon atoms over the course of the simulation emphasizes the peptide insertion and orientation in the DPC micelle and in the POPC bilayer (Figure 4). The periodicity of both curves is characteristic of a helical secondary structure, with 3 to 4 residues per helix turn. The amplitude of the curves is smaller in DPC (~3 Å) than in POPC (~6 Å). This difference could be due to the use of CMAP correction in the case of the simulation of the peptide-DPC micelle system [35]. For both systems, the peptide is buried inside the interface below the polar head group characterized by N and P mean positions (dashed lines on Figure 4). A detailed analysis reflects that the peptide is lying parallel to the interface plane and much deeper inserted in the POPC bilayer than in the DPC micelle. As a matter of fact, the distance between the mean position of the helix axis and the phosphorus mean position is 7.1 Å and 2.3 Å in POPC and DPC respectively.

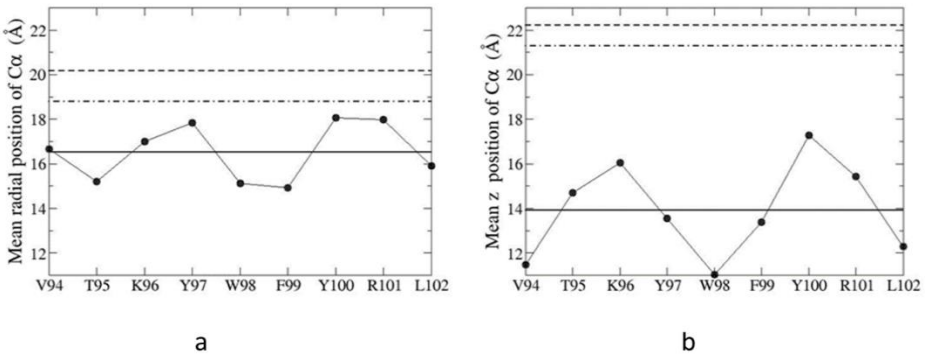

Figure 4. Mean radial position of peptide α-carbon atoms in the DPC micelle (a) and in the POPC bilayer (b) over the course of the simulation (●). The mean axis of the helix (solid line), the mean radial position of the phosphorus (–·–·) and nitrogen (---) atoms are also represented.

The orientation of the peptide backbone is quite similar in both systems, with the buried helical face comprising the α-carbon atoms of W98, F99, L102 and the opposite face exposing to the interface the α-carbon atoms of K96, Y100, R101. Differences essentially concern the α-carbon atoms of V94, T95, Y97 i.e. V94 and Y97 Cα are buried in the POPC bilayer whereas they are exposed to the interface in the DPC micelle and, T95 Cα is exposed to the interface in the POPC bilayer but buried in the DPC micelle. These differences are due to the small variations of the number of residues per helix turn.

3.3. Peptide contacts with lipids

Contacts of the peptide side chains with DPC and POPC are shown in Supplementary Figures S3 and S4. Different atoms of the lipids as well as three different segments of the acyl chains have been considered to allow a detailed analysis of the contacts with the peptide side chains (see Experimental section). Comparison of Supplementary Figures S3 and S4 points out that peptide contacts with DPC are numerous but with short lifetimes and long distances (many small blue dots) whereas peptide contacts with POPC are few but with longer lifetimes and shorter distances (few very large red dots). The number of lipids in contact with the peptide is 20 out of 121 POPC (i.e. 17 % of POPC molecules) in the upper leaflet of the bilayer. On the contrary, 40 out of 50 DPC (i.e. 80 % of DPC molecules) are in contact with the peptide. Moreover, the contact maps are similar for all selected atoms of DPC. Surprisingly, no difference can be established between the three different segments of the acyl chain (Supplementary Figure S3 panels C, D and E) although the peptide is lying at the micelle interface. In contrast, two different types of contact maps appear in the case of POPC: Supplementary Figure S4 panels B, C, D, G display long lifetime and short distance contacts while Supplementary Figure S4 panels A, E, F, H, I display short lifetime and long distance contacts. In the POPC bilayer, the peptide is in close contact with the phosphorus atoms, the glycerol groups and with only the first region of the lipid tails, in agreement with its location much below the interface.

Almost all residues make contact with DPC molecules but, as previously mentioned, these contacts are characterized by long distances and short lifetimes. Nevertheless, there is one exception, DPC24 exhibits particularly short distance and long life contacts with the peptide. These contacts involve essentially the phosphate group and the acyl chain of DPC24 with the side chains of Y97, W98, R101 and L102 (Figure 5 and Supplementary Figure S3).

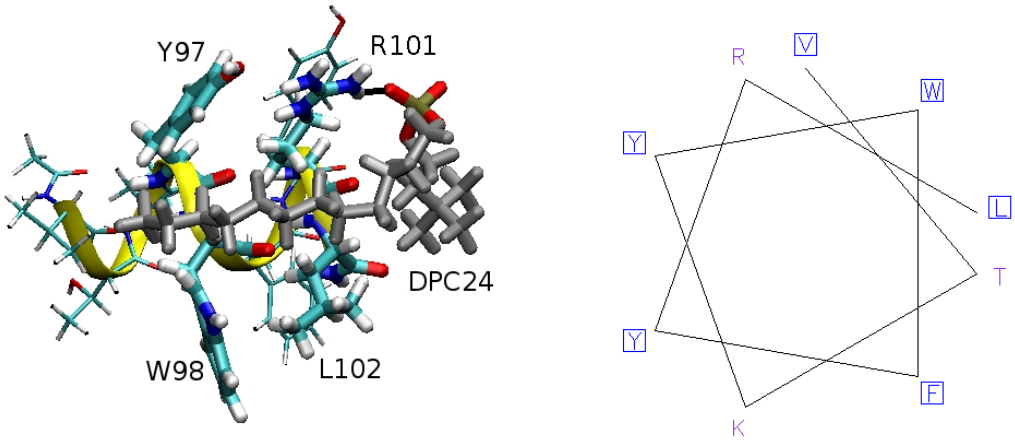

Figure 5. Snapshot from MD simulation of the peptide-DPC micelle system showing DPC24 lying parallel and close to the peptide (view from inside the micelle taken at 36 ns) and the helical wheel representation of the peptide constructed using the online pepwheel tool (https://www.bioinformatics.nl/cgi-bin/emboss/pepwheel - accessed on 29.06.2023): yellow - peptide ribbon; sticks - peptide residues; licorice - Y97, W98, R101, L102 residues; grey and licorice - DPC24; red and yellow, licorice - DPC24 phosphate group; white - hydrogen; cyan - carbons; red - oxygen; blue - nitrogen; black line - hydrogen-bond between an oxygen atom of the DPC24 phosphate group and a hydrogen of the R101 guanidium group.

DPC24 is initially far away from the peptide and becomes close after 15 ns and stays lying parallel to the peptide for further 30 ns. The distance between DPC24 phosphorus atom and R101 ε-carbon atom was monitored over the course of the simulation (Figure 6.a). The distance remains stable at ~ 5 Å from 15 ns to 45 ns. In fact, a hydrogen bond was found between an oxygen atom of the DPC24 phosphate group and a hydrogen atom of the guanidium group of the R101 positively charged side chain for this interval of time (black line in Figure 5). Moreover, from 15 ns to 45 ns, the distance between C27 atom of the DPC24 acyl chain and L102 γ-carbon atom is also stable around 5 Å (Figure 6.b) as a consequence of stable hydrophobic interactions between aliphatic groups of DPC24 acyl chain and L102 side chain.

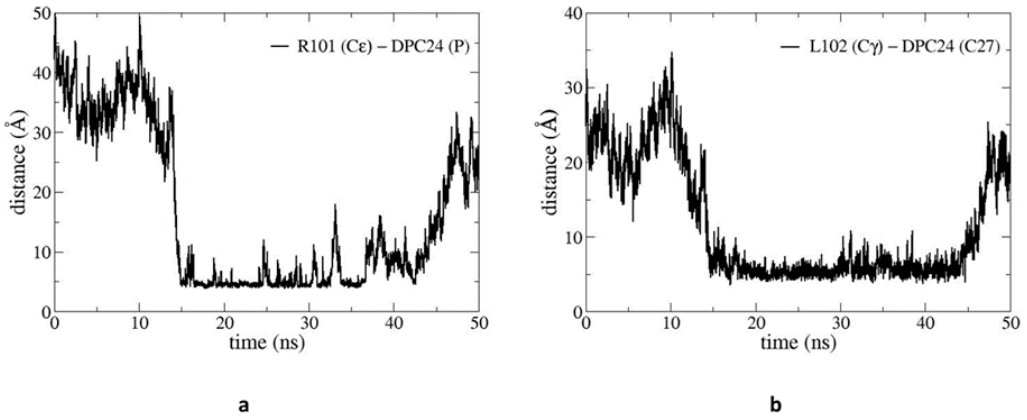

a b

Figure 6. Time evolution of selected distances between the peptide and DPC atoms: (a) distance between R101 ε-carbon atom and DPC24 phosphorus atom; (b) distance between L102 γ-carbon atom and DPC24 C27 atom.

In the case of the bilayer, four lipids (POPC34, POPC41, POPC53 and POPC86) are involved in short distance and long lifetime contacts with peptide side chains (Supplementary Figure S4). In particular, the phosphate and the glycerol groups are involved in these contacts as well as to a less extend the first acyl chain segments (including the first to the seventh methylene groups). The side chain residues in contacts with the phosphate and glycerol groups are T95, F99 and R101, whereas residues V94, W98, F99 and L102 are in contacts with the acyl chains. The contact of W94 with the acyl chain is in good correlation with its known effects in cell-penetrating peptides internalization [41]. However, among the lipids in contact with the peptide, POPC86 makes shorter distance and long lifetime contacts with peptide side chains than the other ones. Indeed, the main interaction between the peptide and the POPC involves R101 side chain and POPC86 head group (Figure 7).

After 12 ns, R101 ε-carbon atom comes close (~ 5 Å) to POPC86 phosphorus atom and remains close until the end of the trajectory (Figure 8.a). This short distance is due to a hydrogen bond between an oxygen atom of the POPC86 phosphate group and a hydrogen atom of the guanidium group of the R101 positively charged side chain. It has to be noticed that contacts were also found between L102 γ-carbon atom and C36 atom of the POPC86 palmitoyl chain (acyl chain second segment) during the last 30 ns of the simulation (see red dots on Supplementary Figure S4 panel E and Figure 8.b).

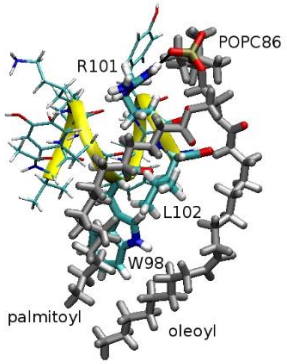

Figure 7. Snapshot from MD simulation of the peptide-POPC bilayer system showing POPC86 in contact with the peptide (in the plane of the membrane at 40 ns): yellow - peptide ribbon; sticks - peptide residues; licorice - W98, R101, L102 residues; grey and licorice - POPC86; red and yellow, licorice - POPC86 phosphate group; white - hydrogen; cyan - carbon; red - oxygen; blue - nitrogen; black line - hydrogen-bond between an oxygen atom of the POPC86 phosphate group and a hydrogen of the R101 guanidium group.

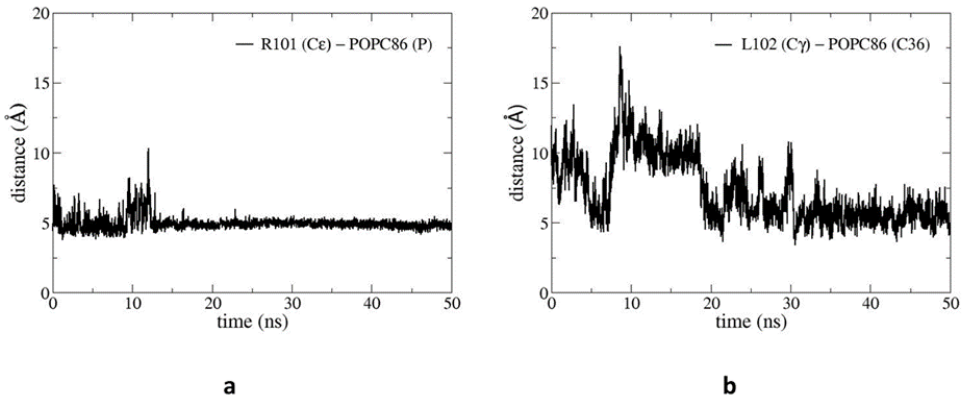

Figure 8. Time evolution of selected distances between the peptide and POPC atoms: (a) distance between R101 ε-carbon atom and POPC86 phosphorus atom; (b) distance between L102 γ-carbon atom and POPC86 C36 atom.

This study reports a detailed comparative analysis of the structural and dynamical characteristics of a POPC bilayer and a DPC micelle. Structural analysis of these membrane mimetics are in agreement with published data. The comparison between the DPC micelle and the POPC bilayer presented in this study reveals some similarities such as: i) the orientation of the head groups, the P-N vectors are parallel to the micelle or the bilayer interfaces, ii) the hydrophobic core size value of 37.6 Å for the DPC micelle versus 41 Å for the POPC bilayer and iii) the almost extended conformations adopted by the saturated chains i.e. DPC acyl and POPC palmitoyl chains (Figure 2).

However, numerous differences between the two membrane mimetics were found. The POPC chains are aligned along the bilayer normal whereas the DPC chains, although being almost extended, experience all directions: from the radial direction to the exposition of one face of the DPC chain to the water (Figure 1). The consequence of this particular arrangement of the DPC chains is a hydrophobic surface twice as large for the DPC micelle as for the POPC bilayer. We also showed that oleoyl chains can adopt curled conformations owing to the great number of defects along the chain and to the presence of the *cis* double bond conformation. Moreover, DPC molecules have a high mobility within the micelle as 80% of DPC are in close contact with the peptide at a given time all over the time course of the simulation. In contrast, only 17 % of POPC molecules make close contacts with the peptide in the bilayer. The intrinsic mobility of DPC molecules inside the micelle is also illustrated by DPC24. Indeed, at the beginning of the simulation, DPC24 phosphorus atom is about 45 Å away from the peptide R101 ε-carbon atom and after 15 ns comes in close contact to the peptide (Figure 6.a).

To further compare the two systems, the interactions of a small interfacial peptide with the DPC micelle and the POPC membrane were studied. For the two systems simulations, the starting structure and position of the peptide were the same and derived from experimental data [20]. The obtained data reveal that the helical structure and the orientation of the peptide parallel to the interface are unchanged during the course of the simulation. The major difference between the two systems is the insertion of the peptide which is more buried inside the bilayer than in the micelle. Similar results have been obtained concerning the insertion of the influenza hemagglutinin fusion peptide in DPC micelle and POPC bilayer [6]. The difference that was observed can be correlated to the difference of the hydrophobic surfaces i.e. the bilayer surface is less hydrophobic than the micelle surface leading to a deeper insertion of the peptide in bilayer in order to accommodate the aromatic and hydrophobic side chains. In micelle, numerous DPC molecules make contact with the peptide and the whole acyl chain is involved. These observations reflect the dynamical behavior of the DPC molecules in the micelle. As a matter of fact, DPC have a high mobility in the micelle and DPC chains experience all directions as already mentioned. In contrast, in the bilayer, few POPC make contact with the peptide and only the phosphate, glycerol and first acyl chains segments are concerned. These results are in agreement with the alignment of the POPC chains along z-axis and an interfacial positioning of the peptide.

The 2-dimensional contact maps (Supplementary Figures S3 and S4) are very informative tools as they allowed to evaluate the proximities between the peptide and the DPC or POPC molecules and to highlight specific contacts. Indeed, mainly two types of contacts are revealed: on the one hand, short lifetime and long distance contacts (small blue dots), characterizing non-specific interactions and on the other hand, long lifetime and short distance contacts (very large red dots). The latter are hallmarks of specific interactions such as hydrogen bonds between acceptor and donor pairs.

In both simulations, similar specific interactions were found between the peptide and a DPC or a POPC molecule (DPC24 in micelle and POPC86 in bilayer). Despite the different environments, the interactions involve the same residues of the peptide and equivalent atoms of the DPC or POPC molecules. A hydrogen bond is found between a hydrogen atom of the guanidium group of R101 side chain and an oxygen atom of the DPC24 or POPC86 phosphate group. The distance between the centers of mass of L102 side chain and of the first acyl chain segment of DPC24 or POPC86 (palmitoyl chain) is small and indicates hydrophobic contacts between the hydrocarbon chains. Comparison of Figures 6.a and 8.a shows similar positioning of the DPC24 acyl chain and the POPC86 palmitoyl chain with respect to the peptide at least for the first carbons of the

palmitoyl chain. Indeed, the DPC or POPC chains seem to accommodate along the hydrophobic face of the peptide mainly defined by L102 and W98 residues. The longest palmitoyl chain reorients after 6 carbons with its chain end parallel to the z-axis. It has to be emphasized that it is the first time that similar specific interactions are observed between a peptide and a DPC or a POPC molecule within two different systems i.e. a micelle and a bilayer by MD simulations. Moreover, the interactions between the peptide and the DPC in micelle were observed despite the high mobility of DPC molecules. This result illustrates that indeed specific interactions between peptide and lipids and/or detergents can be conserved in membrane models such as DPC micelles.

4. Conclusions

The comparison between the DPC micelle and the POPC bilayer using molecular dynamics simulations revealed that: i) the interface hydrophobic surface is twice as large for micelle as for bilayer, ii) the main conformation of DPC and POPC saturated chains is almost extended and, iii) DPC chains explore all the directions while POPC chains are well aligned along z-axis. Moreover, the systems are very different in terms of dynamics. DPC molecules are highly mobile in the micelle in contrast to POPC in bilayer at the time scale of the simulation performed in the present study. The peptide secondary structure and orientation is not strongly influenced by the membrane model. The peptide is much more deeply inserted in the bilayer than in micelle. The contacts between the peptide and the DPC or POPC molecules differ significantly. All atoms of all DPC make short lifetimes and long distances contacts with the peptide in correlation with the DPC dynamics and orientations in micelle. In contrast, few POPC molecules make long lifetimes and short distances contacts with the peptide and these contacts essentially involve their phosphate, glycerol groups and first acyl chains segments. However, despite these differences, similar specific interactions were found in both systems and concern a DPC or a POPC molecule with R101 and L102 side chains.

Conflict of interest

The authors declare no conflict of interest.

Acknowledgements

All calculations were performed thanks to the allocation of time by the French organization “Grand Equipement National de Calcul Intensif” (GENCI)on the large scale facilities of the “Très Grand Centre de Calcul“ (TGCC) of the CEA.

Supplementary material

Figure S1 gives the chemical structure and heteroatoms numbering of DPC and POPC, their atomic structures and the structures of DPC and POPC, respectively. Figure S2 shows the radial distributions of different atoms of DPC molecules over the course of the simulation. Figures S3 and S4 display the 2-dimensional contact maps between peptide side chains and DPC or POPC.

References

[1]. D.E. Warschawski, A.A. Arnold, M. Beaugrand, A. Gravel, E. Chartrand, I. Marcotte, Choosing membrane mimetics for NMR structural studies of transmembrane proteins, Biochimica et Biophysica Acta - Biomembranes 1808 (2011) 1957-1974. DOI: 10.1016/j.bbamem.2011.03.016

[2]. M. Eeman, M. Deleu, From biological membranes to biomimetic model membranes, Biotechnology, Agronomy, Society and Environment 14 (2010) 719-736 (https://popups.uliege.be/1780-4507/index.php?id=17134&file=1&pid=6568)

[3]. N. Kucerka, M.P. Nieh, J. Katsaras, Fluid phase lipid areas and bilayer thicknesses of commonly used phosphatidylcholines as a function of temperature, Biochimica et Biophysica Acta 1808 (2011) 2761–2771. DOI: 10.1016/j.bbamem.2011.07.022

[4]. T.M. Ferreira, F. Coreta-Gomes, O.H.S. Ollila, M.J. Moreno, W.L.C. Vaz, D. Topgaard, Cholesterol and POPC segmental order parameters in lipid membranes: solid state 1H–13C NMR and MD simulation studies, Physical Chemistry and Chemical Physics 15 (2013) 1976-1989. DOI: 10.1039/C2CP42738A

[5]. R.C. Oliver, J. Lipfert, D.A. Fox, R.H. Lo, S. Doniach, L. Columbus, Dependence of micelle size and shape on detergent alkyl chain length and head group, PLOS One 8 (2013) e62488. DOI: 10.1371/journal.pone.0062488

[6]. P. Lague, B. Roux, R.W. Pastor, Molecular dynamics simulations of the influenza hemagglutinin fusion peptide in micelles and bilayers: conformational analysis of peptide and lipids, Journal of Molecular Biology 354 (2005) 1129-1141. DOI: 10.1016/j.jmb.2005.10.038

[7]. H. Saito, T. Morishita, T. Mizukami, K. Nishiyama, K. Kawaguchi, H. Nagao, Molecular dynamics study of binary POPC bilayers: molecular condensing effects on membrane structure and dynamics, Journal of Physics Conference Series 1136 (2018) 012022. DOI: 10.1088/1742-6596/1136/1/012022

[8]. S. Faramarzi, B. Bonnett, C.A. Scaggs, A. Hoffmaster, D. Grodi, E. Harvey, B. Mertz, Molecular dynamics simulations as a tool for accurate determination of surfactant micelle properties, Langmuir 33 (2017) 9934-9943. DOI: 10.1021/acs.langmuir.7b02666

[9]. J.L. Lorieau, J.M. Louis, A. Bax, The complete influenza hemagglutinin fusion domain adopts a tight helical hairpin arrangement at the lipid:water interface, Proceedings of the National Academy of Sciences USA 107 (2010) 11341-11346. DOI: 10.1073/pnas.1006142107

[10]. M. Adélaïde, E. Salnikov, F. Ramos-Martín, C. Aisenbrey, C. Sarazin, B. Bechinger, N. D'Amelio, The mechanism of action of SAAP-148 antimicrobial peptide as studied with NMR and

molecular dynamics simulation, Pharmaceutics 15 (2023) 761. DOI:10.3390/pharmaceutics15030761

[11]. L. Zhao, Z. Cao, Y. Bian, G. Hu, J. Wang, Y. Zhou, Molecular Dynamics Simulations of Human Antimicrobial Peptide LL-37 in Model POPC and POPG Lipid Bilayers, International Journal of Molecular Sciences 19 (2018) 1186. DOI: 10.3390/ijms19041186

[12]. A. Isvoran, P. Nedellec, V. Beswick, A. Sanson, Study of the electrostatic interactions between peptides and lipids at the membranes interface by molecular dynamics simulation, Revue Roumaine de Chimie 51 (2006) 1019-1024 (https://revroum.lew.ro/wp-content/uploads/2006/RRC_10_2006/sumar.pdf)

[13]. L.O. Nunes, V.H.O. Munhoz, A.A. Sousa, K.R de Souza, T.L. Santos, M.P. Bemquerer, D.E.C. Ferreira, M.T.Q. de Magalhães, J.M. Resende, A.F.C. Alcântara, C. Aisenbrey, D.P. Veloso, B. Bechinger, R.M. Verly, High-resolution structural profile of hylaseptin-4: Aggregation, membrane topology and pH dependence of overall membrane binding process, Biochimica et Biophysica Acta. Biomembranes 1863 (2021) 183581. DOI: 10.1016/j.bbamem.2021.183581

[14]. S. Ghosh, G. Pandit, S. Debnath, S. Chatterjee, P. Satpati, Effect of monovalent salt concentration and peptide secondary structure in peptide-micelle binding, RSC Advances, 11 (2021) 36836. DOI: 10.1039/D1RA06772A

[15]. A.P. Lyubartsev, A.L. Rabinovich, Recent development in computer simulations of lipid bilayers, Soft Matterials 7 (2011) 25-39. DOI: 10.1039/C0SM00457J

[16]. A. Isvoran, D. Craciun, A. Ciorsac, N. Perrot, V. Beswick, P. Nedellec, A. Sanson, N. Jamin, A bioinformatics study concerning structural and functional properties of human caveolin proteins, Journal of the Serbian Chemical Society 79 (2014) 133-150. DOI: 10.2298/JSC130716100I

[17]. A.W. Cohen, R. Hnasko, W. Schubert, M.P. Lisanti, Role of caveolae and caveolins in health and disease, Physiological Reviews 84 (2004) 1341-1379. DOI: 10.1152/physrev.00046.2003

[18]. H. Li, V. Papadopoulos, Peripheral-type benzodiazepine receptor function in cholesterol transport. Identification of a putative cholesterol recognition/interaction amino acid sequence and consensus pattern, Endocrinology 139 (1998) 4991-4997. DOI: 10.1210/endo.139.12.6390

[19]. R.M. Epand, B.G. Sayer, R.F. Epand, Caveolin scaffolding region and cholesterol-rich domains in membranes, Journal of Molecular Biology 345 (2005) 339-350. DOI: 10.1016/j.jmb.2004.10.064

[20]. C. Le Lan, J. Gallay, M. Vincent, J.M. Neumann, B. de Foresta, N. Jamin, Structural and dynamic properties of juxta-membrane segments of caveolin-1 and caveolin-2 at the membrane interface, European Biophysical Journal 39 (2010) 307-325. DOI: 10.1007/s00249-009-0548-4

[21]. J. Lipfert, L. Columbus, V. B. Chu, S.A. Lesley, S. Doniach, Size and shape of detergent micelles determined by small-angle X-ray scattering, Journal of Physical Chemistry B 111 (2007) 12427-12438. DOI: 10.1021/jp073016l

[22]. D.P. Tieleman, D. van der Spoel, H.J.C. Berendsen, Molecular dynamics simulations of dodecylphosphocholine micelles at three different aggregate sizes: micellar structure and chain relaxation, Journal of Physical Chemistry B 104 (2000) 6380-6388. DOI: 10.1021/jp001268f

[23]. S. Abel, F. Y. Dupradeau, M. Marchi, Molecular dynamics simulations of a characteristic DPC micelle in water, Journal of Chemical Theory and Computation 8 (2012) 4610-4623. DOI: 10.1021/ct3003207

[24]. S.J. Lee, B. Olsen, P.H. Sehlesinger, N.A. Baker, Characterization of perfluorooctylbromide-based nanoemulsion particles using atomistic molecular dynamics simulations, Journal of Physical Chemistry B 114 (2010) 10086-10096. DOI: 10.1021/jp103228c

[25]. N. Kucerka, S. Tristram-Nagle, J.F. Nagle, Structure of fully hydrated fluid phase lipid bilayers with monounsaturated chains, Journal of Membrane Biology 208 (2005) 193-202. DOI: 10.1007/s00232-005-7006-8

[26]. J. Seelig, Deuterium magnetic resonance: theory and application to lipid membranes, Quarterly Reviews of Biophysics10 (1977) 353-418. DOI: 10.1017/s0033583500002948

[27]. B.R. Brooks, C.L. Brooks, A.D. Mackerell Jr., L. Nilsson, R.J. Petrella, B. Roux, Y. Won, G. Archontis, C. Bartels, S. Boresch, A. Caflisch, L. Caves, Q. Cui, A.R. Dinner, M. Feig, S. Fischer, J. Gao, M. Hodoscek, W. Im, K. Kuczera, T. Lazaridis, J. Ma, V. Ovchinnikov, E. Paci, R.W. Pastor, C.B. Post, J.Z. Pu, M. Schaefer, B. Tidor, R.M. Venable, H.L. Woodcock, X. Wu, W. Yang, D.M. York, M. Karplus, CHARMM: the biomolecular simulation program, Journal of Computational Chemistry 30 (2009) 1545-1614. DOI: 10.1002/jcc.21287

[28]. A.D. MacKerell, D. Bashford, M. Bellott, R.L. Dunbrack, J.D. Evanseck, M.J. Field, S. Fischer, J. Gao, H. Guo, S. Ha, D. Joseph-McCarthy, L. Kuchnir, K. Kuczera, F.T.K. Lau, C. Mattos, S. Michnick, T. Ngo, D.T. Nguyen, B. Prodhom, W. E. Reiher, B. Roux, M. Schlenkrich, J.C. Smith, R. Stote, J. Straub, M. Watanabe, J. Wiorkiewicz-Kuczera, D. Yin, M. Karplus, All-Atom empirical potential for molecular modeling and dynamics studies of proteins, Journal of Physical Chemistry B 102 (1998) 3586-3616. DOI: 10.1021/jp973084f

[29]. J.B. Klauda, R.M. Venable, J.A. Freites, J.W. O'Connor, D.J. Tobias, C. Mondragon-Ramirez, I. Vorobyov, A.D. MacKerell, R.W. Pastor, Update of the CHARMM all-atom additive force field for lipids: validation on six lipid types, Journal of Physical Chemistry B 114 (2010) 7830-7843. DOI: 10.1021/jp101759q

[30]. W.L. Jorgensen, J. Chandrasekhar, J.D. Madura, R.W. Impey, M.L. Klein, Comparison of simple potential functions for simulating liquid water, Journal of Chemical Physics 79 (1983) 926-935. DOI: 10.1063/1.445869

[31]. V. Beswick, A. Isvoran, P. Nedellec, A. Sanson, N. Jamin, Membrane interface composition drives the structure and the tilt of the single transmembrane helix protein PMP1: MD studies, Biophysical Journal 100 (2011) 1660-1667. DOI: 10.1016/j.bpj.2011.02.002

[32]. J.P. Ryckaert, G. Ciccotti, H.J.C. Berendsen, Numerical integration of the Cartesian equations of motion of a system with constraints: molecular dynamics of n-alkanes, Journal of Computational Physics 23 (1977) 327-341. DOI: 10.1016/0021-9991(77)90098-5

[33]. J. Lauterwein, C. Bosch, L.R. Brown, K. Wuthrich, Physicochemical studies of the protein-lipid interactions in melittin-containing micelles, Biochimica and Biophysica Acta 556 (1979) 244-264. DOI: 10.1016/0005-2736(79)90046-4

[34]. T.A. Darden, L.G. Pedersen, Molecular modelling: an experimental tool, Environmental Health Perspectives 101 (1993) 410-412. DOI: 10.1289/ehp.93101410

[35]. A.D. MacKerell Jr., M. Feig, C.L. Brooks, Improved treatment of the protein backbone in empirical force fields, Journal of America Chemical Society 126 (2004) 698-699. DOI: 10.1021/ja036959e

[36]. M.R. Saviello, S. Malfi, P. Campiglia, A. Cavalli, P. Grieco, E. Novellino, A. Carotenuto, New insight into the mechanism of action of the temporin antimicrobial peptides, Biochemistry 49 (2010) 1477-1485. DOI: 10.1021/bi902166d

[37]. X. Cheng, S. Jo, H.S. Lee, J.B. Klauda, W. Im, CHARMM-GUI micelle builder for pure/mixed micelle and protein/micelle complex systems, Journal of Chemical Information and Modeling 53 (2013) 2171-2180. DOI: 10.1021/ci4002684

[38]. T. Lazaridis, B. Mallik, Y. Chen, Implicit solvent simulations of DPC micelle formation, Journal of Physical Chemistry B 109 (2005) 15098-15106. DOI: 10.1021/jp0516801

[39]. L. Saiz, M.L. Klein, Influence of highly polyunsaturated lipid acyl chains of biomembranes on the NMR order parameters, Journal of American Chemical Society 123 (2001) 7381-7387. DOI: 10.1021/ja003987d

[40]. M. Wojciechowska, J. Miszkiewicz, J. Trylska, Conformational changes of anoplin, W-MreB1-9, and (KFF)3K peptides near the membranes, International Journal of Molecular Sciences 21 (2020) 9672. DOI: 10.3390/ijms21249672

[41]. S. Khemaissa, A. Walrant, S. Sagan, Tryptophan, more than just an interfacial amino acid in the membrane activity of cationic cell-penetrating and antimicrobial peptides, Quarterly Reviews of Biophysics 55 (2022) E10. DOI: 10.1017/S0033583522000105

Received: 05.09.2023
Received in revised form: 05.12.2023
Accepted: 09.12.2023